Clays and Clay Minerals, Vol. 41, No. 5, 570–579, 1993.

DIAGENETIC KAOLINITE/DICKITE (BETIC CORDILLERAS, SPAIN)

M. D. Ruiz Cruz and L. Moreno Real

Departamento de Química Inorgánica, Cristalografía y Mineralogía,
Facultad de Ciencias, 29071, Málaga, Spain

Abstract—The lower Permo-Triassic sediments of the Maláguide Complex contain abundant dickite. Whole rocks were studied by optical microscopy, scanning electron microscopy, and X-ray powder diffraction. The 2–20 μm and <2 μm size fractions were extracted and analyzed by scanning and transmission electron microscopy, X-ray powder diffraction, infrared spectroscopy, differential thermal analysis, and thermogravimetry.

In the coarse-grained samples, the 2–20 μm size fraction consisted of well-crystallized dickite associated with minor quantities of kaolinite, illite, quartz, and hematite. XRD patterns of the fine-grained samples and the <2 μm fractions showed the existence of well-crystallized minerals in which several reflections of dickite (11*l*, 02*l*) were absent and the 132/13$\bar{2}$ reflections were shifted. These patterns suggest the presence of an intermediate member between well-crystallized dickite and well-crystallized kaolinite. Only locally high-order reflections are present at 10.5 Å and 18–22 Å. DTA and IR data agree with those from XRD.

The observed compositional and structural variations are a function of the lithology and the particle size of the sample. The sequence kaolinite → kaolinite/dickite → dickite is proposed for the development of these materials during Alpine metamorphism.

Key Words—Crystallinity, Dickite, Differential thermal analysis, Electron microscopy, Infrared spectroscopy, Interstratified minerals, Kaolinite, Thermogravimetry, X-ray powder diffraction.

INTRODUCTION

Disorder in kaolinite has been extensively investigated (Brindley and Robinson, 1946; Murray and Lyons, 1959; Hinckley, 1963; Mitra, 1963; Noble, 1971; Plançon and Tchoubar, 1977; Gomes, 1987; Drits and Tchoubar, 1990). X-ray patterns reveal the increasing disorder such that: 1) The basal reflections 001 and 002 become broader and less intense; 2) The sequence of 02*l* and 11*l* reflections become weak and broad; 3) The reflections 13*l* and h0*l*, which form two groups of triplets in ordered kaolinites, become less well defined (Brindley, 1980).

By contrast, dickite has received little attention. Usually, hydrothermal and sedimentary dickite appear to be structurally well-ordered and morphologically well-formed. Nevertheless, Brindley and Porter (1978) found a wide range of order-disorder in dickites from Jamaica. X-ray patterns reported by these authors show that the transition from well-ordered to disordered dickites is indicated, as in kaolinites, by the weakening and broadening of the reflections 11*l* and 02*l* (in the range 20–34° 2θ) and of the two doublets h0*l* and 13*l* (in the range 34–40° 2θ). Reflections with k ≠ 3n are the most affected. The highly disordered samples are very similar to disordered kaolinites as shown by Brindley and Robinson (1946).

Disorder in dickite can be interpreted in the same way as kaolinite (Plançon and Zacharie, 1990), i.e., in terms of displacement of Al vacancies. In a mixture of kaolinite and dickite stacking arrangements, the average α-angle should be intermediate between 91.8° and 90° (Brindley, 1980). Consequently, X-ray patterns should show a certain degree of triclinicity. Therefore, the magnitude of the resolution between 1$\bar{3}$1 and 131 in kaolinite can be considered as a triclinicity index (Gomes, 1987) or a monoclinicity measure (Plançon and Tchoubar, 1977).

On the other hand, intercalation of hydrazine into the layer space in kaolinite or dickite is strongly influenced by structural disorder (Range *et al.*, 1969). While well-ordered minerals yield intercalation compounds rapidly and quantitatively (after treatment the basal spacing reaches 10.4 Å), disordered minerals contain fractions that do not react. Thus, intercalation reactions might be used to quantify the disorder in kaolinites (Cases *et al.*, 1986) and, presumably, in dickites.

Infrared spectra for kaolinite and dickite are also different. According to data by Farmer (1974), the spectrum of kaolinite shows four bands at 3697, 3669, 3652, and 3620 cm^{-1}. The spectrum of dickite shows three bands with different intensity ratios that are slightly shifted with respect to kaolinite (3704, 3654, and 3622 cm^{-1}). Disordered kaolinites produce intermediate bands. Thus, differences in the position, shape, and relative intensities of the bands can be used to determine the existence of kaolinite, dickite and their mixtures (Farmer and Russell, 1964; Lombardi *et al.*, 1987; Prost *et al.*, 1989).

Typical DTA curves for dickite have endotherms ranging from broad peaks at 500°–700°C to sharp peaks near 700°C. The peak temperatures for kaolinite range from 550°–580°C (Mackenzie, 1970). Differences in the temperature of these dehydroxylation peaks are attrib-

uted frequently to variations in the degree of structural order (Smikatz-Kloss, 1974), but also the differences could be an index to detect kaolinite/dickite interstratifications (Brindley and Porter, 1978).

In the present work, several techniques were used to study diagenetic dickites. The results define the degree of order-disorder present and can be used to suggest an origin for these structures.

MATERIALS AND METHODS

The samples investigated belong to two detrital sedimentary sequences located in the lowest Permo-Triassic of the Malaguide Nappe (Internal zones, Betic Cordilleras, Spain: Figure 1A). In Figure 1B, the location of the eight samples used in the present paper are indicated. These samples have been selected from 60 studied in a previous mineralogical analysis of several profiles of this formation. The selected samples represent a wide range of grain size, from conglomeratic sandstones to silty clays (Ruiz Cruz and Puga, 1992).

Whole rock samples were analyzed by X-ray powder diffraction (XRD), scanning electron microscopy (SEM), and polarizing microscope (PM). The <2 μm and 2–20 μm size fractions were separated by sedimentation and analyzed by XRD, infrared spectroscopy (IR), differential thermal analysis (DTA), thermogravimetry (TGA), and transmission electron microscopy (TEM).

A Siemens-501 diffractometer with CuKα radiation and graphite monochromator was operated at 35 mA, 40 kV, step size = 0.01° 2θ, and counting time = 2 s. Locations of the peaks were determined with a DACO-MP computer using the least square approximation of 3rd degree to the given intensities; the second derivative of each data point was then computed from the 3rd degree polynomials associated with this point. Resolution of the method for locating peaks is better than 0.01 Å for the range investigated.

Semiquantitative determination of the mineral composition of the whole-rock samples was carried out using random powder mounts and the intensity factors of Schultz (1964). Semiquantitative analysis of the 2–20 μm and <2 μm fractions was accomplished with oriented mounts on glass slides, following the method and the intensity factors of Islam and Lotse (1986). Routine treatments with ethylene glycol (EG) and dimethylsulphoxide (DMSO) and heating at 550–650°C for two hours were systematically performed. Dickite and chlorite were differentiated according to the acid treatment method of Martín Vivaldi and Rodriguez Gallego (1961). The hydrazine test was performed on oriented samples (Range *et al.*, 1969).

Characterization of dickite in 2–20 μm and <2 μm fractions was performed on unoriented samples. To obtain random orientation, freeze-drying procedures were used. The 002/060 and 004/060 intensity ratios were measured to evaluate the degree of orientation (Brindley and Kurtossy, 1961).

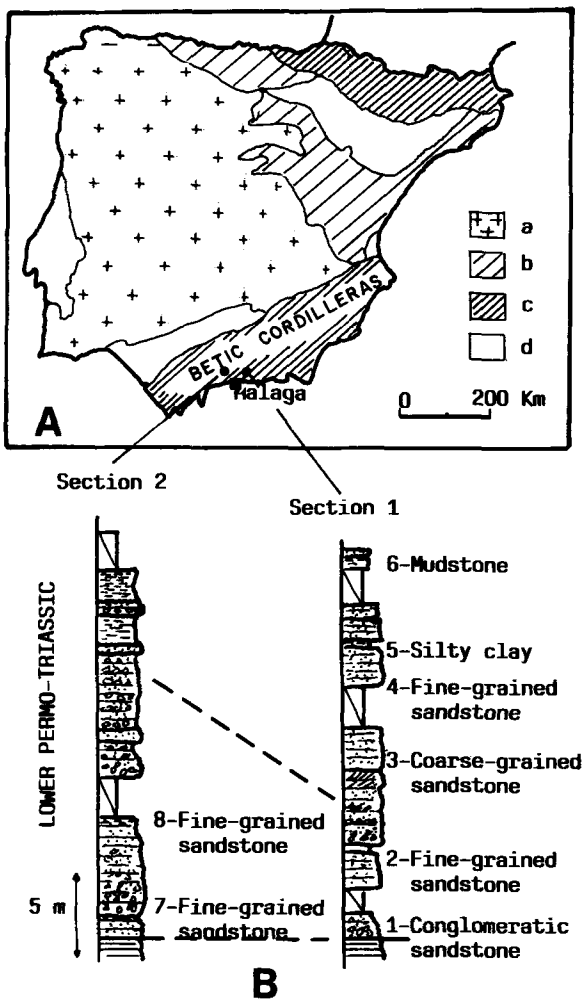

Figure 1. A) Geologic sketch map of the Iberian Peninsula and location of analzyed sections where a = Iberian Massif, b = Alpine Borders, c = Alpine Cordilleras, and d = Neogene Basins. B) Location and lithology of samples cited.

Specific measurements included: 1) the angular half-height width and asymmetry of the 002 and 004 reflections (Gomes, 1987); 2) the intensities and resolution of the 20°–40° 2θ range reflections (Plançon and Zacharie, 1990); and 3) the exact position of 13*l* reflections (Plançon and Zacharie, 1990) calculated using the 102 peak of quartz as an internal standard. We have used, as an approximate parameter, the intensity ratio $I_{110+}I_{112}/I_{11\bar{1}\text{-}020}$ (similar to Hinckley index in kaolinites) to estimate disorder in dickites. Estimation of the interference of illite on the 11$\bar{1}$-020 dickite reflections was evaluated from the ratio $I_{110\text{-}11\bar{1}}/I_{11\bar{4}}$ of the illite reflections, obtained from an illite-rich sample (Sample 6). Only the 110-11$\bar{1}$, 20$\bar{2}$, and 133 illite reflections can interfere with dickite reflections. Thus,

https://doi.org/10.1346/CCMN.1993.0410507 Published online by Cambridge University Press

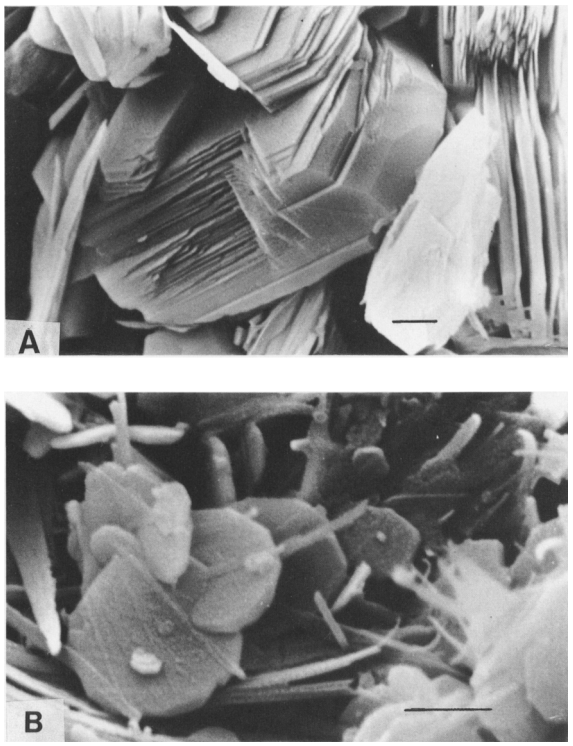

Figure 2. Scanning electron micrographs of dickites. A) Coarse-grained dickite showing a high degree of compactation. B) Platy hexagonal particles present in finest fractions. Scale bar = 1 μm.

the dickite reflections used in disorder measures (002, 110, 11$\bar{2}$, 132, and 13$\bar{2}$) are not affected by the presence of illite.

Point-counting was undertaken to quantify the detrital mineral content, the abundance of cement, and the porosity. The morphology, composition, and textural relations of the minerals were studied with a Jeol JSM-840 scanning electron microscope and a Jeol STEM-100 CXII transmission electron microscope equipped with an energy-dispersive X-ray analyser (EDX). SEM examinations were carried out on fractured surfaces of specimens after critical point drying and coating with gold. Samples for TEM were prepared by dispersing the <2 μm and 2–20 μm fractions in water and allowing a small drop to dry on separate specimen support grids.

Infrared spectra of the 2–20 μm and <2 μm fractions were recorded over the range 4000–240 cm^{-1} on a Perkin-Elmer spectrophotometer using KBr discs containing 2 wt. % of sample. The spectra were obtained at room temperature. The influence of illite in IR spectra was estimated from the spectrum of the illitic sample (Sample 6), which shows a single band at 3635 cm^{-1}. The bands at higher frequencies are exclusively due to a dickite-type mineral.

Differential thermal analysis and thermogravimetry were carried out on a Rigaku Thermoflex TAS 100 with samples of 35–40 mg, heated at 10°C/min. The influence of illite in these curves can be estimated from the curve of the illitic sample (Sample 6). This curve offers two weak endothermic peaks at 60° and 520°C. The endothermic peaks between 530° and 670°C are not affected by the presence of illite.

RESULTS

In the lower Permo-Triassic sediments, several lithotypes were distinguished: conglomerates, sandstones, siltstones, and mudstones. Conglomeratic sandstones and fine to medium-grained sandstones are made up of quartz and minor amounts of feldspar, muscovite, and rock fragments. The detrital matrix (<30 μm) is illitic, with the dominant polytype being $2M_1$. Sandstones are cemented by dickite, hematite, and minor dolomite. Locally, zeolitic cement has been identified. Neoformed muscovite and chlorite were also observed in some of the sequences. Silty clays contain quartz, illite, chlorite, and kaolinite/dickite as main components. The chemical composition of neoformed muscovite and chlorite allowed us to deduce that these materials were submitted to very low grade metamorphism (Ruiz Cruz and Puga, 1992).

Dickite showed variable textural and morphologic characteristics. In coarse-grained samples, pore-filling dickite occurs as well-developed crystals generally 1 to 2 μm thick and compacted plates (Figure 2A) with sizes >5 μm, Vermicular dickite is also present. These textures suggest compacted crystal growth. Frequently, intergrown quartz-dickite was observed. In silty clays and in the finest fractions of sandstones and conglomerates, well-developed hexagonal plates with sizes 1–2 μm occurred. They appeared to be locally illitized (Figure 2B).

X-ray powder diffraction

Table 1 shows the values of the "Hinckley-type index," corrected to eliminate the influence of illite. The range of values in the 2–20 μm fraction is greater than in the <2 μm fraction, and it appears to be related to lithologic variations such as median grain size and % matrix.

Defect-free dickite is the dominant phyllosilicate in the 2–20 μm size-fraction of sandstones (Table 2). Figure 3A shows the XRD patterns (19.5°–40° 2θ) for this fraction from five dickite-rich samples (1–5) and an illitic-rich sample (6). The 110 and 11$\bar{2}$ peaks were well developed, especially in Samples 1 and 3. The d-value for the 132 peak was 2.324–2.327 Å for Samples 1 to 4, and the 13$\bar{2}$ peak was 2.515–2.518 Å. Sample 4 showed dickite and kaolinite reflections (11$\bar{1}$, 021, 022, and 1$\bar{3}$1). Sample 5 showed several features that are important to point out: 1) the absence of the 11*l* and 02*l* reflections of dickite except for the 11$\bar{2}$

https://doi.org/10.1346/CCMN.1993.0410507 Published online by Cambridge University Press

Table 1. Hinckley-type index of two size-fractions.

Sample	2–20 μm	<2 μm
1	1.47	0.47
2	1.04	0.28
3	2.71	0.62
4	1.56	0.28
5	0.56	0.47
7	1.62	0.55
8	0.89	0.36

reflection; 2) the enhancement of the $13\bar{2}$ reflection; and 3) the shift from 2.324 to 2.332 Å for the 132 reflection. The pattern did not correspond to disordered kaolinite (Brindley and Robinson, 1946) or to disordered dickite (Brindley and Porter, 1978).

XRD patterns of the <2 μm size-fraction (Figure 3B) were very similar to those in the 2–20 μm fraction of Sample 5. The position of the 132 reflection changed to 2.330–2.335 Å. The $13\bar{2}$ peak was located at 2.522–2.527 Å. The influence of illite on these patterns can be illustrated from Sample 6 (Figure 3A), which corresponds to 2–20 μm fraction of a quartz-illite mudstone with a minor amount of dickite. Only the 110-

Table 2. Lithologic characteristics and variation of the clay minerals in 2–20 μm and <2 μm fractions.

Sample	Median grain size (mm)	% matrix (<0.003 mm)	Mineralogical composition (wt. %) 2–20 μm D	I	Ch	<2 μm K/D	I	Ch
1	3.5–0.31	15.5	71	29	—	38	62	—
2	0.12	21.1	58	42	—	22	78	—
3	0.34	6.2	86	14	—	43	57	—
4	0.10	24.5	51	49	—	35	65	—
5		64.8	25	57	18	20	73	7
6		>90	—	100	—	8	92	—
7	0.13	25.8	66	34	—	47	53	—
8	0.12	20.7	39	61	—	24	76	—

D = Dickite. I = Illite. Ch = Chlorite. K/D = Kaolinite/dickite mixed-layers.

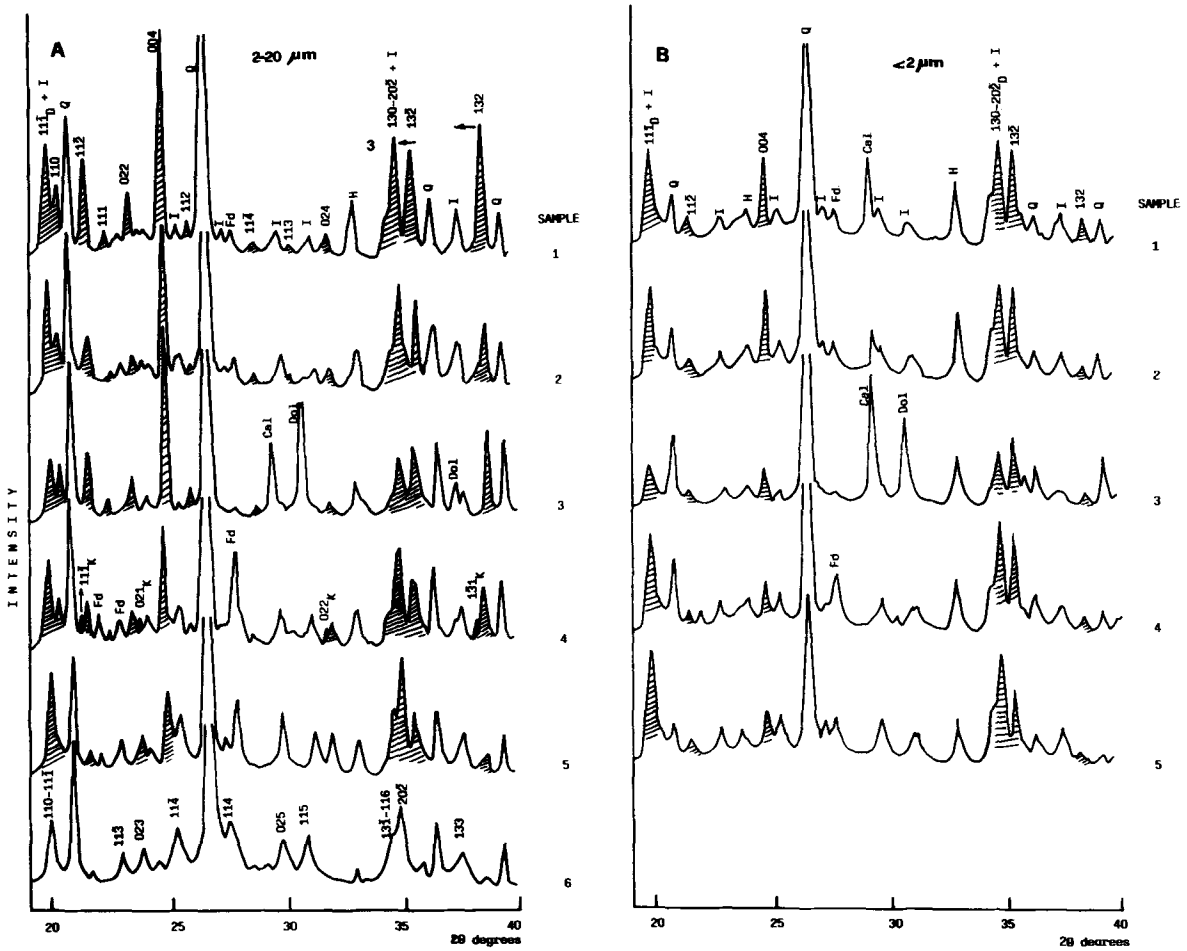

Figure 3. XRD patterns (19,5–40° 2θ) of randomly oriented A) 2–20 μm and B) <2 μm size fractions. Numbers correspond to sample locations shown in Figure 1. Striped peaks belong to dickite. Blackened peaks belong to kaolinite. Arrows indicate the direction of the peak shifts. D = Dickite. K = Kaolinite. I = Illite. Q = Quartz. Fd = Feldspar. Cal = Calcite. Dol = Dolomite. H = Hematite.

https://doi.org/10.1346/CCMN.1993.0410507 Published online by Cambridge University Press

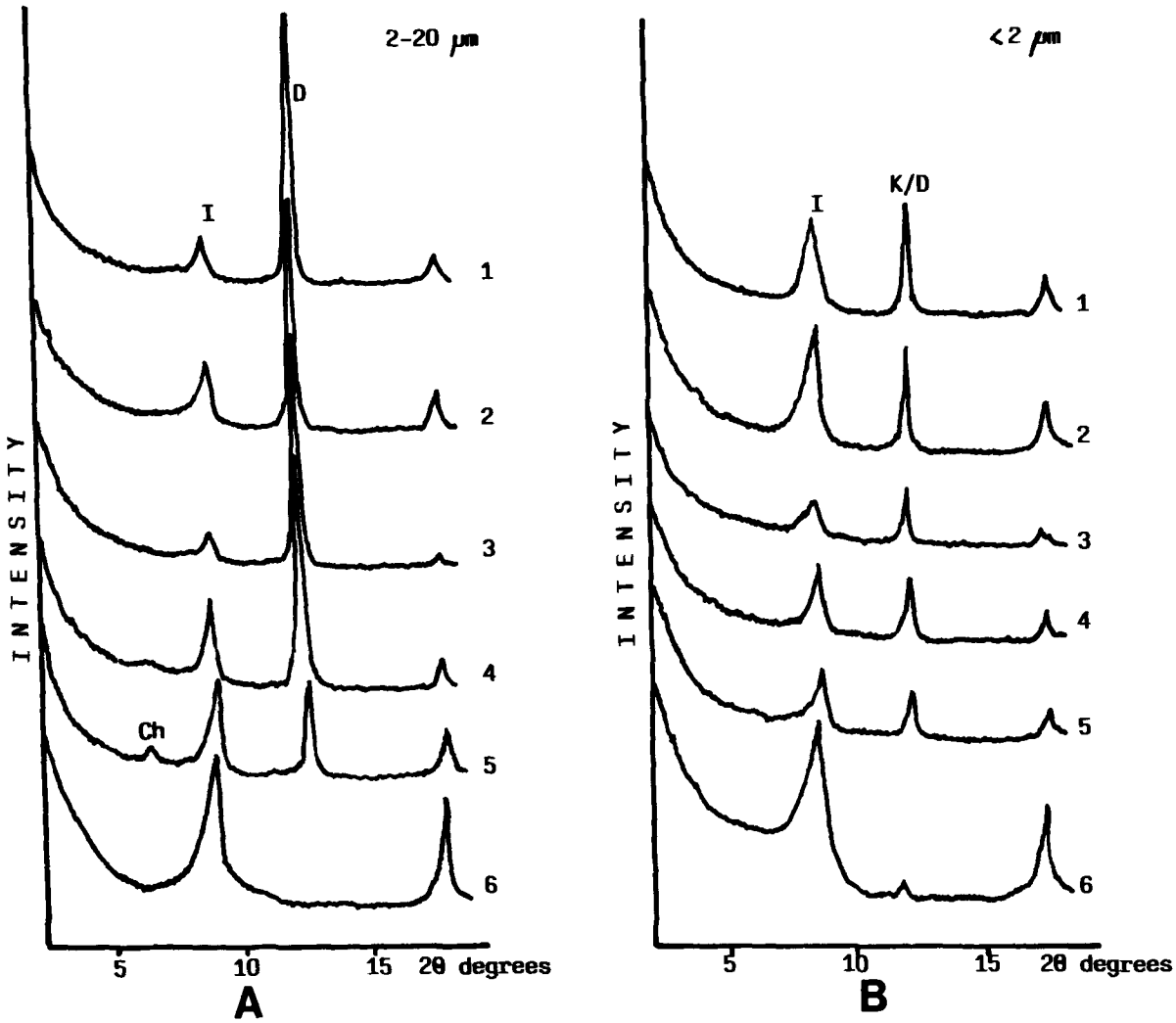

Figure 4. XRD traces of the air-dried oriented mounts of the A) 2–20 μm and B) <2 μm size fractions. Numbers correspond to sample locations shown in Figure 1. D = Dickite. I = Illite. Ch = Chlorite. K/D = kaolinite/dickite mixed-layers.

$11\bar{1}$, $20\bar{2}$, and 133 illite reflections can interfere with dickite reflections. The influence of kaolinite is clearly reflected in the value of the Hinckley-type index (Table 1) for the 2–20 μm fraction of Sample 4 due to the enhancement of the 110 reflection and the presence of the $11\bar{1}$ kaolinite peak.

Inspection of the 2–15° 2θ range showed that the position and asymmetry of the 12.4° peak did not change as a function of particle size fraction or lithology (Figure 4). The shape and width of this peak are characteristic of well-ordered minerals. The small influence of the particle size is shown by the slightly broader peaks in the <2 μm fraction.

Hydrazine treatment permits the detection of the differently ordered components of kaolinite and dickite (Range *et al.*, 1969). Most of the samples analyzed gave an intercalation compound with a basal spacing of 10.3–10.4 Å (Figure 5A). This reaction is characteristic of materials with no, or relatively little, disorder.

However, in several samples belonging to Section 2 (Figure 1), the 2–15° 2θ range showed weak reflections beside the 10 Å illite peak at 10.3–10.6 Å and at 18–22 Å that cannot be ascribed to illite (Figures 5B and 5C). EG treatment and heating at 550°C for 2 hr indicate the absence of smectite or chlorite-type layers that could produce these reflections. Hydrazine treatment (Figure 5B) causes the shift of the 10.3 Å reflection toward lower angles and the complete shift of the 7Å reflection to 10.4 Å, confirming the absence of intercalation disorder. In spite of the 10.4 Å reflection overlap with the 10 Å illite reflection, the effect is notably sharper than in the air-dried sample. Dimethylsulphoxide solvation (Figure 5C) produced an incomplete shift of the 7.1 Å reflection to 11.2 Å and a

https://doi.org/10.1346/CCMN.1993.0410507 Published online by Cambridge University Press

remarkable sharpening of the 10 Å reflection. The behaviour of the 10.3–10.6 Å reflection indicates the presence of a randomly interstratified kaolinite/dickite mixed-layer mineral.

Infrared spectra

The IR spectra of both size-fractions for selected samples are illustrated in Figure 6. Differences in composition are shown by the position and the relative intensities of the absorption bands in the OH-stretching region (3800–3500 cm^{-1}). In all spectra, the intensity of the 3660 cm^{-1} bands relative to the 3700 cm^{-1} band indicated the presence of a dickite-type mineral (Farmer, 1974). Spectra 1, 2, 3, and 4 (Figure 6A) are indicative of defect-free dickite and contain intense bands at 3720–3710, 3660, and 3630 cm^{-1}. In Spectrum 4, the existence of a weak peak at 3703 cm^{-1} might indicate the presence of some kaolinite. Spectrum 5 (Figure 6A) and all spectra of the <2 μm fractions (Figure 6B) show a variable shift of the highest frequency band from 3710 to 3695 cm^{-1}. In these spectra, two doublets at 3660–3650 cm^{-1} and 3638–3630 cm^{-1} were visible. The influence of illite in these spectra is only apparent by the enhancement of the 3630 cm^{-1} band in contrast to that in Figure 6A.

Thermal analyses

DTA curves of both size-fractions from selected samples are shown in Figure 7. In the DTA curves of the 2–20 μm fractions, the main endothermic dehydroxylation peak ranged from 555°C to 670°C (Figure 7A). Its shape and width indicated the existence of well-ordered dickite (Sample 3). Diagrams 1 and 2 (Figure 7A) are very similar to those reported by Brindley and Porter (1978) for well-ordered dickite.

In the finest fractions, the temperature of the main endothermic peak ranged from 520° to 634°C. Only the peaks observed at 60° and 520°C could be enhanced by illite as can be deduced from the curve of the illitic sample (Sample 6, Figure 7A). The shape and the peak temperature of the endothermic peak in Curves 1, 2 and 4 of Figure 7B are similar to those reported by Brindley and Porter (1978) for disordered dickite.

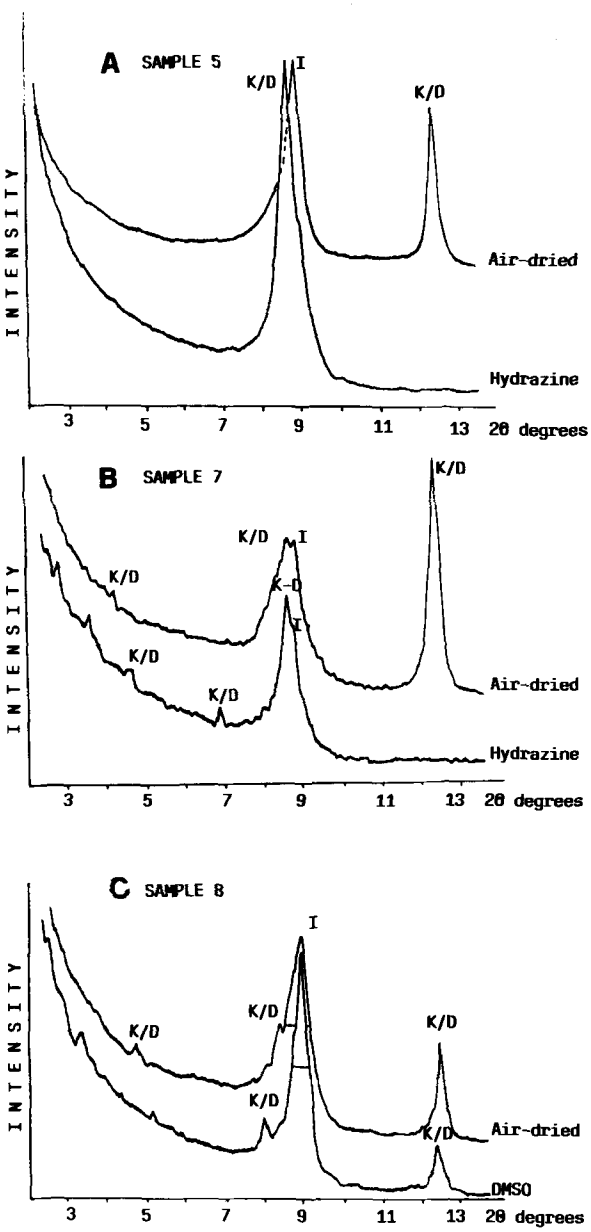

Figure 5. A) and B) XRD traces of the air-dried and hydrazine-treated oriented mounts. Samples 5 and 7, <2 μm size fraction. C) XRD traces of the air-dried and dimethylsulphoxide-solvated oriented mounts. Sample 8, <2 μm size fraction. IC = Illite crystallinity. I = Illite. K/D = Kaolinite/dickite mixed-layers.

DISCUSSION

In this work we have used several analytical techniques to determine the nature and degree of order in sedimentary dickites.

Although IR spectra are not determinative, they permit us to observe differences in structural characteristics of the analyzed dickites. In the spectra of <2 μm fractions the shift (to 3695 cm^{-1}) of the highest frequency band and the presence of several bands in the range 3685–3630 cm^{-1} allows us to suggest the existence of kaolinite-like configurations within the dickite structure (Lombardi *et al.*, 1987; Prost *et al.*, 1989). In interstratified lamellar structures, successive layers and interlayer spaces have different structures. Therefore, dickite/kaolinite interstratifications should have specific IR spectra due to, at the molecular scale, their structural-OH groups having different configurations.

DTA provides additional information. Differences between the 2–20 μm fraction and the <2 μm fraction diagrams could be attributed to variations in the degree of structural order in dickites (Mackenzie, 1970; Brin-

https://doi.org/10.1346/CCMN.1993.0410507 Published online by Cambridge University Press

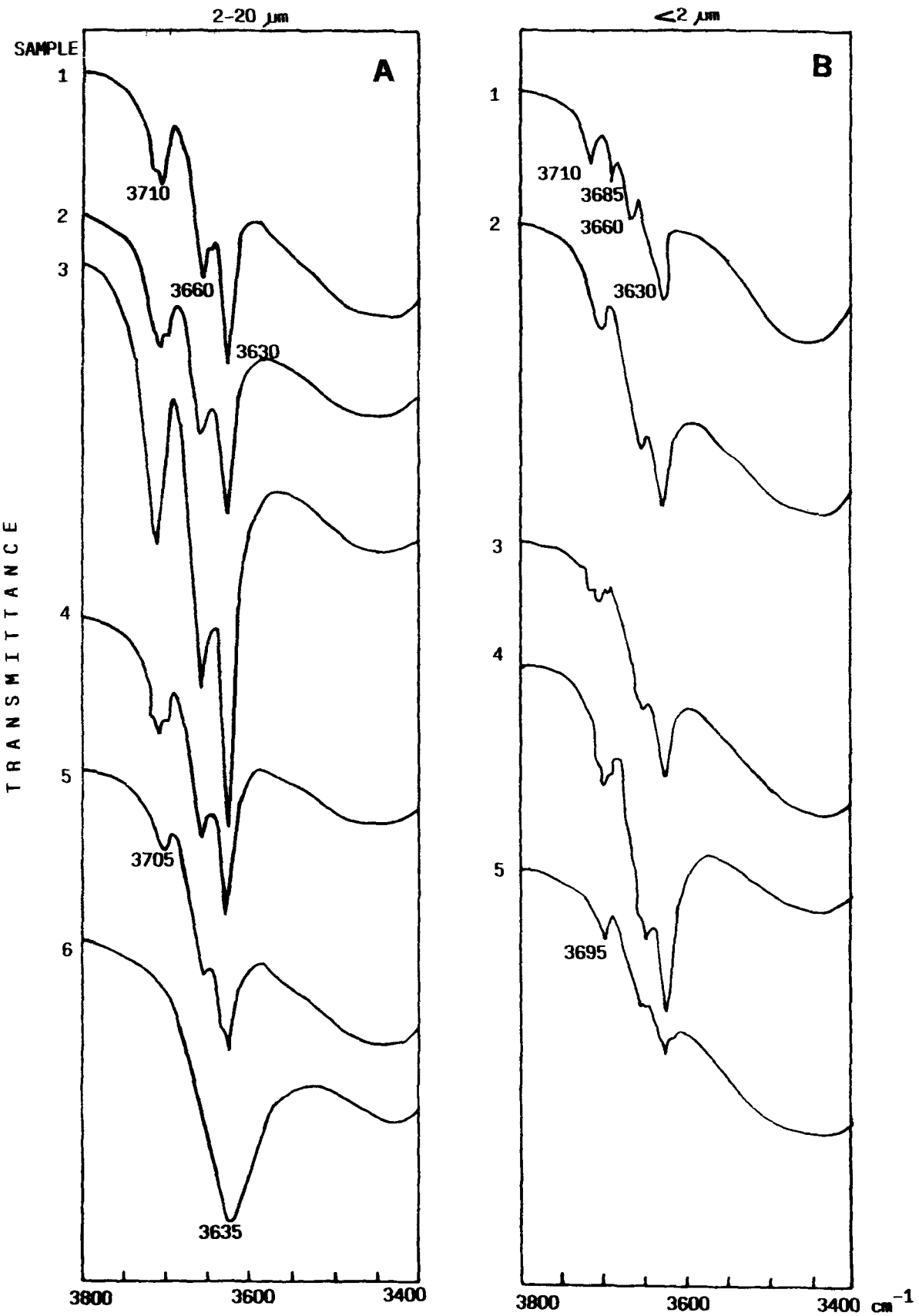

https://doi.org/10.1346/CCMN.1993.0410507 Published online by Cambridge University Press

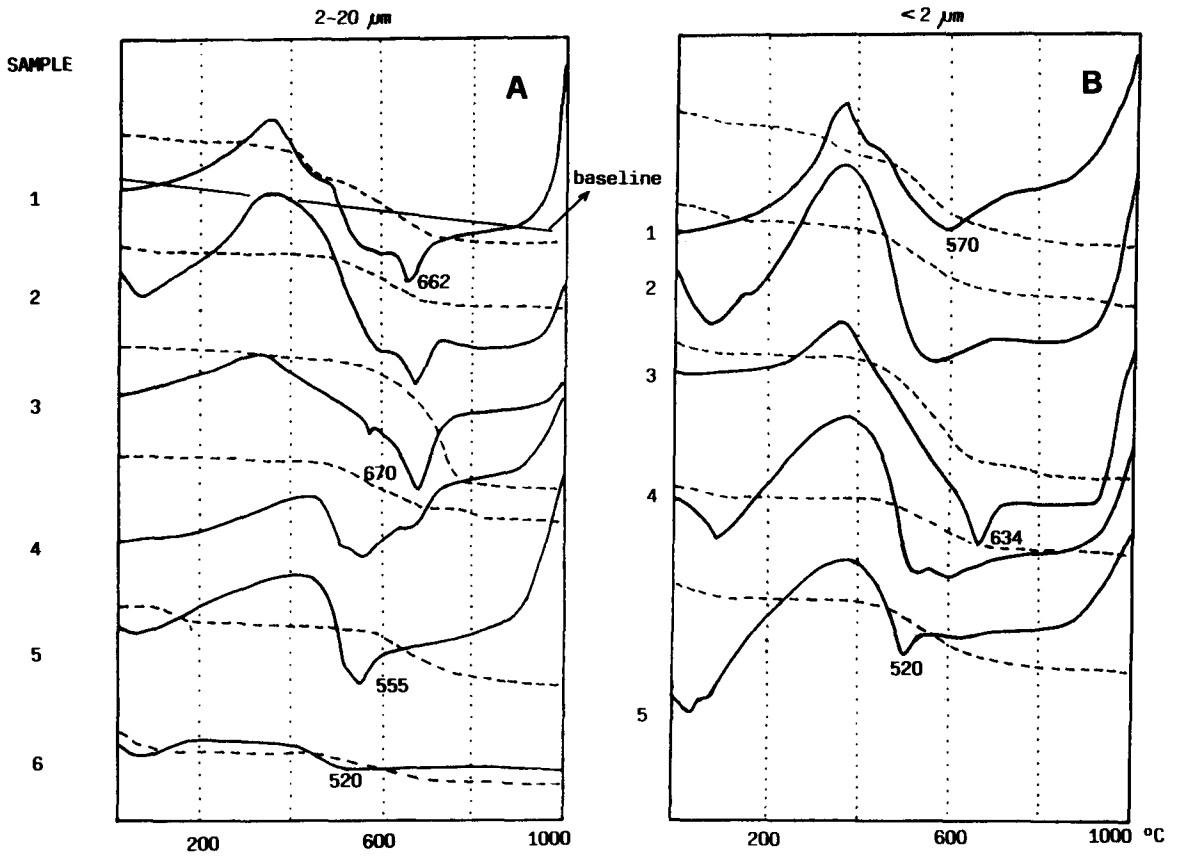

Figure 7. Differential thermal analysis and thermogravimetric curves of the A) 2–20 μm and B) <2 μm size fractions. Numbers refer to samples from locations shown in Figure 1. In curve 1A, the baseline has been drawn.

dley and Porter, 1978) as a function of particle size, but Curve 5 (Figure 7A) and Curve 3 (Figure 7B) are important exceptions. They suggest instead the existence of kaolinite/dickite arrangements with different proportions of both components as suggested by Stoch (1964). The peak temperature of dehydroxylation indicates the approximate proportion of kaolinite in the kaolinite/dickite mixed-layered material.

XRD provides the best results to infer the existence of kaolinite/dickite interstratifications with reasonable accuracy. The observed differences in the 20–40° 2θ range of the powder diagrams could be attributed to the presence of planar defects, as in kaolinite or to existence of mixed-layers dickite/kaolinite. Both types of disorder yield powder diagrams showing important departures from the diffractogram of perfect structures if the interstratification is irregular (Drits and Tchoubar, 1990). But the characteristics of the 001/002 reflection and their behaviour after hydrazine treatment as well as the persistence of several reflections (i.e., $11\bar{2}$), indicate the existence of well-ordered phases, randomly stacked. The presence of quartz in these samples made it possible to determine if the 131 reflection of kaolinite is present, but the shift of the 132 and $13\bar{2}$ peaks suggests that the two components of the structural sequence (dickite and kaolinite) diffract coherently. The magnitude of these shifts can be considered as an indication of the unit cell symmetry (Brindley, 1980; Plançon and Zacharie, 1990). A good correlation also exists between the temperature of the main endothermic peak in DTA curves and the position of the 132 and $13\bar{2}$ reflections in XRD patterns (Figure 8).

The presence of an interstratified phase is usually confirmed by the positions of the basal reflections. In this case both end-members have similar values of d_{00l}; consequently, the peak positions are little affected by composition. The intensity and position of 001′, 002′, etc., reflections are only dependent on end-member proportion and on the regularity of the sequence. The high-order reflections (near 10.5 and 21 Å) are excep-

←

Figure 6. Infrared spectra of the A) 2–20 μm and B) <2 μm size fractions. Numbers refer to samples from locations shown in Figure 1.

https://doi.org/10.1346/CCMN.1993.0410507 Published online by Cambridge University Press

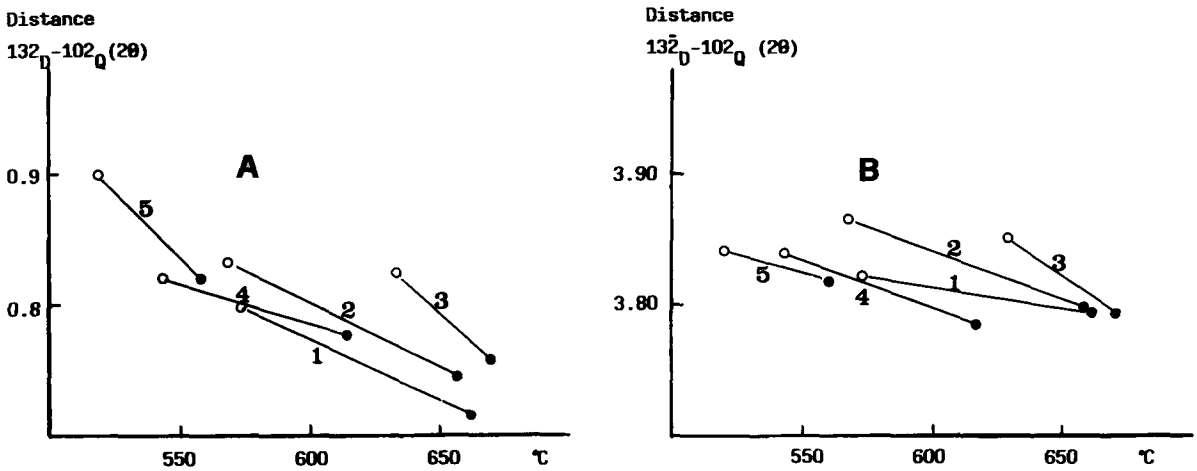

Figure 8. Relation between the shift of the A) 132 reflections and B) 13$\bar{2}$ reflections plotted against the temperature of the main endothermic peak from DTA. Dots = 2–20 μm samples. Open circles <2 μm samples.

tional in the samples studied and would indicate the presence of a slightly ordered K/D interstratified mineral. Nevertheless, in most cases these reflections are absent, suggesting the presence of random interstratification.

The structural variation of these minerals is a function of the lithology, especially of the pore and particle-size and percent of detrital matrix (Table 2). Kaolinite cement developed extensively in sandstones as a consequence of feldspar and mica dissolution (Ruiz Cruz and Puga, 1992). Dickite cement is usually related to burial (Dunoyer de Segonzac, 1969; Kantorowicz, 1984; Chamley, 1990). In the zone studied, the Permo-Triassic sediments have been slightly buried, but pressures approximating 2–3 Kb were experienced. We suggest a transformation in the direction kaolinite → kaolinite/dickite → dickite, which developed during the first stage of Alpine metamorphism simultaneous to development of metamorphic chlorites and micas. The transformation has been more complete in the coarser, better sorted sandstones.

CONCLUSIONS

Data from IR and DTA agree with those from XRD and reveal the existence of kaolinite/dickite interstratifications in the Betic Permo-Triassic. These interstratified minerals are characterized as follows:

1) The position of the highest frequency band in their spectra is intermediate between well-crystallized dickite and kaolinite. Several bands are present in 3660–3630 cm^{-1} range.
2) The dehydroxylation endothermic peaks are broad and asymmetric and range from 520° to 600°C.
3) XRD patterns are characterized by the disappearance of 11*l* and 02*l* reflections of dickite and a shift toward larger angles for the 132 and 13$\bar{2}$ peaks. In certain cases, high-order reflections (at 21–22 Å and 10.3–10.5 Å) are present.

REFERENCES

Brindley, G. W. (1980) Order-disorder in clay mineral structures: in *Crystal Structures of Clay Minerals and Their Identification,* G. W. Brindley and G. Brown, eds., London, Mineralogical Society, 125–195.

Brindley, G. W. and Kurtossy, S. S. (1961) Quantitative determination of kaolinite by X-ray diffraction: *Amer. Mineral.* **46,** 1205–1215.

Brindley, G. W. and Porter, A. R. D. (1978) Occurrence of dickite in Jamaica. Ordered and disordered varieties: *Am. Mineral* **63,** 554–562.

Brindley, G. W. and Robinson, K. (1946) Randomness in the structure of kaolinitic clay minerals: *Trans Faraday Soc.* **42B,** 198–205.

Cases, J. M., Cunin, P., Grillet, Y., Poinsignon, C., and Yvon, J. (1986) Methods of analysing morphology of kaolinites: Relations between crystallographic and morphological properties: *Clay Miner.* **21,** 55–68.

Chamley, H. (1990) *Sedimentology:* Springer-Verlag, Berlin and Heidelberg, 285 pp.

Drits, V. A. and Tchoubar, C. (1990) *X-ray Diffraction by Disordered Lamellar Structures:* Springer-Verlag, Berlin and Heidelberg, 371 pp.

Dunoyer de Segonzac, G. (1969) Les minéraux argileux dans la diagènese passage au métamorphism: *Mém. Serv. Carte Géol. Als. Lorr.* **29,** 320 pp.

Farmer, V. C. (1974) *The Infrared Spectra of Minerals:* Mineralogical Society, London, 539 pp.

Farmer, V. C. and Russell, J. D. (1964) The infrared spectra of layer silicates: *Spectrochim. Acta* **20,** 1149–1173.

Gomes, C. S. F. (1987) X-ray diffraction and infrared absorption crystallinity indices in kaolinites. Their significance, capacities and limitations: *Proc. 6th Meet. European Clay Groups, Sevilla (Spain),* E. Galán, J. L. Pérez Rodriguez, and J. Cornejo, eds., 265–269.

Hinckley, D. N. (1963) Variability in "crystallinity" values among the kaolin deposits of the coastal plain of Georgia and South Carolina: *Clays & Clay Minerals* **11,** 229–235.

Islam, A. K. and Lotse, E. G. (1986) Quantitative mineralogical analysis of some Bangladesh soils with X-ray, ion

exchange and selective dissolution techniques: *Clay Miner.* **21,** 31–42.

Kantorowicz, J. (1984) Nature, origin and distribution of authigenic clay minerals from Middle Jurassic Ravenscar and Brent Group sandstones: *Clay Miner.* **19,** 359–375.

Lombardi, G., Russell, J. D., and Keller, W. D. (1987) Compositional and structural variations in the size fractions of a sedimentary and a hydrothermal kaolin: *Clays & Clay Minerals* **35,** 321–335.

Mackenzie, R. C. (1970) Simple phyllosilicates based on gibbsite and brucite-like sheets: in *Differential Thermal Analysis,* R. C. Mackenzie, ed., Academic Press, London and New York, 498–537.

Martín Vivaldi, J. L. and Rodriguez Gallego, M. (1961) Some problems in the identification of clay minerals in mixtures by X-ray diffraction photographs. Part. I. Chlorite-kaolinite mixtures: *Clay Miner.* **4,** 288–292.

Mitra, G. B. (1963) Structure defects in kaolinite: *Z. Kristallogr. Kristallgeom.* **119,** 161–175.

Murray, H. H. and Lyon, S. C. (1959) Correlation of paper-coating quality with degree of perfection of kaolinite: *Clays & Clay Minerals* **4,** 31–40.

Noble, F. R. (1971) Study of disorder in kaolinite: *Clay Miner.* **9,** 71–81.

Plançon, A. and Tchoubar, C. (1977) Part II. Nature and proportions of defects in natural kaolinites: *Clays & Clay Minerals* **25,** 436–450.

Plançon, A. and Zacharie, C. (1990) An expert system for the structural characterization of kaolinites: *Clay Miner.* **25,** 249–260.

Prost, R., Dameme, A., Huard, E., Driard, J., and Leydecker, J. P. (1989) Infrared study of structural OH in kaolinite, dickite, nacrite and poorly crystalline kaolinite at 5 to 600 K: *Clays & Clay Minerals* **37,** 464–468.

Range, K. J., Range, A., and Weiss, A. (1969) Fire-clay type kaolinite or fire-clay mineral? Experimental classification of kaolinite-halloiste minerals: *4th Int. Clay Conf., Tokyo, Vol. 1,* Israel University Press, Jerusalem, 3–13.

Ruiz Cruz, M. D. and Puga, E. (1992) Análisis mineralógico del Permotrías del Complejo Maláguide en los alrededores de Málaga: *Ref. III Congreso de Geología de España y VIII Congreso Latinoamericano de Geología, Salamanca, Vol. III,* Soc. Geol. España, 329–334.

Schultz, L. G. (1964) Quantitative interpretation of mineralogical composition from X-ray and chemical data for Pierre Shale: *Geol. Surv. Prof. Paper* **391-C,** 31 pp.

Smikatz-Kloss, W. (1974) *Differential Thermal Analysis. Applications and Results in Mineralogy:* Springer-Verlag, Berlin, 188 pp.

Stoch, L. (1964) Thermal dehydroxilation of minerals of the kaolinite group: *Bull. Acad. Polonaise Sci.* **12,** 173–180.

(Received 28 January 1992; accepted 24 March 1993; Ms. 2180)